Coseismic ionospheric disturbances triggered by the Chi-Chi earthquake

J. Y. Liu,[1,2] H. F. Tsai,[3] C. H. Lin,[4] M. Kamogawa,[5] Y. I. Chen,[6] C. H. Lin,[7] B. S. Huang,[7] S. B. Yu,[7] and Y. H. Yeh[7]

Received 30 September 2009; revised 3 February 2010; accepted 2 March 2010; published 4 August 2010.

[1] At 17:47 UT on 20 September 1999, a large earthquake of magnitude M_w 7.6 struck the central Taiwan near a small town of Chi-Chi. The ground-based receivers of the global positioning system (GPS) in the Taiwan area detected coseismic ionospheric disturbances (CIDs) in the total electron content (TEC) triggered by the Chi-Chi earthquake. When the CIDs travel away from the origin on the Earth surface and then propagate into the ionosphere, their amplitudes and periods generally become smaller and longer, respectively. Moreover, two global grid searches, adapting the ray-tracing and the beam-forming techniques, have been used to analyze the observed GPS TEC. We have not only estimated the average speed of the CIDs propagating in the atmosphere and ionosphere but also determined the location of CID origin on the Earth surface by using the two techniques. The results show that the observed CIDs result from shock-acoustic waves triggered by sudden and large vertical motions of the Chi-Chi earthquake.

Citation: Liu, J. Y., H. F. Tsai, C. H. Lin, M. Kamogawa, Y. I. Chen, C. H. Lin, B. S. Huang, S. B. Yu, and Y. H. Yeh (2010), Coseismic ionospheric disturbances triggered by the Chi-Chi earthquake, *J. Geophys. Res.*, *115*, A08303, doi:10.1029/2009JA014943.

1. Introduction

[2] The ionosphere can be affected by a variety of disturbances. Natural sources, such as severe weather, volcanic eruption, earthquake, and tsunami, create mechanical disturbances (waves) in the neutral atmosphere and propagate into the ionosphere where they interact with the ionized gas [*Davies*, 1990]. Using the HF (high frequency) Doppler sounding technique, scientists have observed ionospheric disturbances triggered by strong earthquakes [*Davies and Baker*, 1965; *Leonard and Barnes*, 1965; *Row*, 1967; *Yuen et al.*, 1969; *Tanaka et al.*, 1984; *Blanc*, 1985; *Artru et al.*, 2004; *Liu et al.*, 2006a]. Following *Heki and Ping* [2005], the ionospheric disturbances triggered by earthquakes are called as the coseismic ionospheric disturbances (CIDs). Due to limited numbers and distributions of the Doppler sounding stations, it was difficult to examine propagations of the CIDs in detail. Recently, the total electron content (TEC) derived from data recorded by dense ground-based receivers of the global positioning system (GPS) have been employed to examine CIDs excited by earthquakes [*Calais and Minster*, 1995; *Afraimovich et al.*, 2001; *Ducic et al.*, 2003; *Artru et al.*, 2005; *Heki and Ping*, 2005; *Jung et al.*, 2006; *Liu et al.*, 2006b; *Astafyeva and Afraimovich*, 2006; *Otsuka et al.*, 2006; *Astafyeva and Heki*, 2009; *Astafyeva et al.*, 2009].

[3] Several types of CIDs have been identified by their characteristics. The short period (about several tens of seconds but usually less than about 5 minutes) CIDs are induced by Rayleigh (seismic) waves propagating near the Earth's surface with a speed of about 2.6–3.6 km/s [*Yuen et al.*, 1969; *Davies*, 1990; *Ducic et al.*, 2003; *Artru et al.*, 2004; *Liu et al.*, 2006a]. The long period (generally about tens of minutes) CIDs are signatures of acoustic gravity waves [*Davies*, 1990] induced by large vertical surface motions around the epicenter traveling with speeds of about 300 m/s, whereas the velocity of shock-acoustic waves varies from 900 to 1200 m/s [*Afraimovich et al.*, 2001]. The most pronounced and common CIDs are shock acoustic waves propagating upward from the focal area in a narrow cone of zenith angles, which are usually detected 10–20 minutes after strong earthquakes nearby their epicenters [*Calais and Minster*, 1995; *Afraimovich et al.*, 2001; *Heki and Ping*, 2005; *Jung et al.*, 2006]. Meanwhile, sudden vertical displacement of the Earth's surface near an epicenter could excite acoustic gravity waves propagating horizontally with a speed of about 300 m/s with periods of tens of minutes in the lower atmosphere, which can travel for a long

[1]Institute of Space Science, National Central University, Chung-Li, Taiwan.
[2]Center for Space and Remote Sensing Research, National Central University, Chung-Li, Taiwan.
[3]Center Weather Bureau, Taipei, Taiwan.
[4]Department of Earth Science, National Cheng Kung University, Tainan, Taiwan.
[5]Department of Physics, Tokyo Gakugei University, Tokyo, Japan.
[6]Institute of Space Statistics, National Central University, Chung-Li, Taiwan.
[7]Institute of Earth Sciences, Academia Sinica, Taipei, Taiwan.

0148-0227/10/2009JA014943

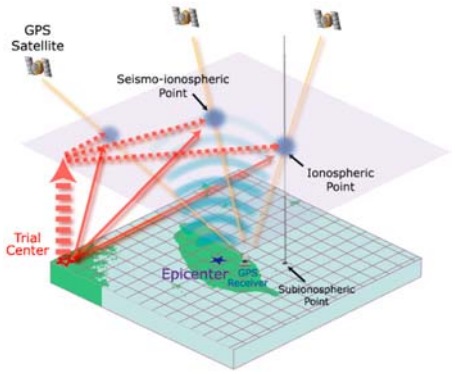

Figure 1. A sketch of using ground-based GPS receivers to monitor seismo-ionospheric disturbances. The solid blue star and the open red star denote the reported epicenter and the trial center, respectively. The triggered disturbances at a trial center travel either vertically into the ionosphere and then horizontally (red dashed arrows) or radially (red solid arrows) into the ionosphere. The orange and shaded lines denote the slant (line-of-sight) total electron content and vertical total electron content, respectively. The blue dotted symbols are the seismo-ionospheric points. A subionospheric point is the down projection of an associated ionospheric point. When the CID arrives at an ionospheric point, the point is termed the SIP.

distance into the ionosphere as giant CIDs [*Bolt*, 1964; *Pokhotelov et al.*, 1995; *Liu et al.*, 2006a; *Astafyeva and Afraimovich*, 2006].

[4] Recently scientists [*Afraimovich et al.*, 2006; *Jung et al.*, 2006; *Liu et al.*, 2006b; *Kiryushkin and Afraimovich*, 2007] develop techniques, algorithms, and models to locate sources and find characteristics of CIDs in the TEC derived from networks of ground-based GPS receivers. In this paper, two global grid searches adapting the ray-tracing technique [*Lee and Lahr*, 1972] (for details, see *Lee and Stewart* [1981]) and the beam-forming technique [*Huang et al.*, 1999], the standard methods used by seismologists, are employed to analyze CIDs recorded by the local ground-based GPS receivers during the 20 September 1999 M_w 7.6 Chi-Chi earthquake.

2. Methodology

[5] The GPS consists of more than 24 satellites, distributed in 6 orbits around the globe at an altitude of 20,200 km. Each satellite transmits two frequencies of signals, 1575.42 and 1227.60 MHz. Since the ionosphere is a dispersive medium, scientists are able to evaluate the ionospheric effects on the radio wave propagation or the corresponding ray path TEC with measurements of the modulations on carrier phases and code pseudo-ranges recorded by dual-frequency receivers (cf., *Sardón et al.*, 1994; *Leick* 1995; *Liu et al.*, 1996). Here, the slant TEC (STEC) between a GPS satellite and a ground-based receiver can be written as

$$\mathrm{STEC} = (1/40.3)[(f_1^2 f_2^2)/(f_1^2 - f_2^2)][(L_1 - L_2) - (d_r + d_s)],$$

where L_1 and L_2 denote the carrier phases of the two frequencies f_1 and f_2, and d_r and d_s are the differential biases for receiver and satellite, respectively. From the broadcast ephemeris (i.e., the satellite time, elevation, location, etc.) and a given ionospheric (shell) height, the slant TEC along the ray path can be converted, usually using a simple cosine function of the satellite zenith, into the vertical TEC (VTEC, for simplicity hereafter, TEC) at its associated longitude and latitude [*Tsai and Liu*, 1999]. Based on *Sardón et al.* [1994], the ionospheric height is assumed at 350 km altitude. To detect temporal changes in the ionosphere, *Liu et al.* [2004, 2006c] introduce a differential TEC (dTEC), which is defined by subtracting each VTEC at $t = i + 1$ from its previous 30 sec value at $t = i$ (i.e., $\mathrm{dTEC}_{i+1/2} = \mathrm{VTEC}_{i+1} - \mathrm{VTEC}_i$, the sampling rate of a standard GPS receiver is 30 sec), and show that the dTEC is proportional to the Doppler (frequency) shift Δf of the GPS signal, which is expressed as

$$\mathrm{dTEC} = (cf/40.3)\Delta f,$$

where c and f are the light speed in free space and the GPS carrier phase frequency. Based on this, the amplitude and period of the CIDs can be evaluated.

[6] The location of a recorded dTEC is defined as the intercept of the ray path of the GPS signal and the ionospheric height, which is termed the ionospheric (pierce) point (Figure 1). For a network of ground-based GPS receivers, we can treat these ionospheric points as space seismometers floating at 350 km altitude of the ionosphere [*Sardón et al.*, 1994] to observe CIDs. When a CID is detected, its arrival time and the location (longitude, latitude, ionospheric height) of the space seismometer (hereafter, the seismo-ionospheric point; SIP) are further recorded.

[7] On the other hand, the ray-tracing technique [*Lee and Stewart*, 1981] and the beam-forming technique [*Huang et al.*, 1999] have been traditionally employed by seismologists to locate an earthquake source (or hypocenter). In the ray-tracing technique, for a given velocity model, scientists guess the location of a hypocenter and calculate the arrival time of seismic waves at each seismometer (the forward calculation). From the difference between the calculated and observed arrival times at the seismometers, a new location of the hypocenter is further issued and tried. When the differences reach the minimum, the iteration process is stopped, and the trial (guess) center is then declared to be the hypocenter. Similarly, scientists can guess the location of a hypocenter but calculate the earthquake onset time from each seismometer (the backward calculation). The minimum in differences of the calculated onset times is the criterion of the hypocenter location determination. By contrast, for a given velocity model, the beam-forming technique [*Huang et al.*, 1999] guesses a hypocenter and computes the speeds and associated standard deviation by dividing the distances between the hypocenter and the seismometers by the differences between the reported onset time and observed arrival times at the seismometers. Similarly, when the standard deviation yields the minimum, the hypocenter is considered to be located.

[8] Here, we adapt the above techniques and construct two global grid searches to find the CID origin on the Earth's surface. Owing to that the velocity model of the atmosphere is not fully understood and developed, we follow Hamilton's Variational Principle of Lagrangian

Mechanics assuming that there are numerous paths between the CID origin (or trial center) and the SIP, which are the two end points of the paths. Note that Hamilton's Variational Principle states that the integral taken along a path of the possible motion of a physical system is an extremum when evaluated along the path of motion that is the one actually taken (for example, see *Fowles and Cassiday* [1999]). Thus, in this study, instead of a velocity model, a possible path for the CID propagation is required to be given in advance. It is obvious that the true propagation path varies from the guess center horizontally propagating along the Earth's surface and then vertically to the SIP, and from the guess center vertically up to 350 km altitude and then horizontally to the SIP. The simulation [*Heki and Ping*, 2005] and observations [*Astafyeva and Afraimovich*, 2006] show that the CIDs generally travel away from the disturbance origin on the Earth's surface to the ionosphere in the radial direction. For simplicity, a two-segment path (the CIDs traveling from the guess center vertically up to 350 km altitude and then horizontally to the SIPs) and a great circle path (the CIDs at the guess center traveling radially to the SIPs) are examined (see Figure 1).

[9] Our ray-tracing technique using the backward calculation obtains the travel time from a trial center (or grid point) to each SIP point with the given path, derives the onset times at the trial center by subtracting the calculated travel times from the observed arrival times of the CIDs at the SIPs, and then computes the mean value of the derived onset times and the associated standard deviation (Figure 1). In the two-segment path, for each SIP, we calculate the onset time at the trial center by

$$T_{Ck} = T_{Ak} - (D_{Vk}/VV + D_{Hk}/V_H),$$

where T_{Ak} is the arrival time recorded by the kth SIP, D_{Vk} is 350 km altitude, D_{Hk} is the horizontal distance of the SIP to the trial center, and V_V and V_H are the average vertical and horizontal speeds, respectively. Since there are 14 SIPs, we therefore calculate the average onset time and associated standard deviation, std, for each trial center. We repeat this procedure through the whole grid points (trial centers) and draw contours of the standard deviations to find the minimum, which is considered as the disturbance origin on the Earth surface. Here, the trial center lies between 18°N and 28°N and 116°E and 126°E. The 0.1° spatial resolution in both the longitude and latitude gives 10,000 points (= 100 × 100) of the trial center. To find the optimal onset time and the CID origin, various values of the average vertical speed V_V and horizontal speed V_H are tested.

[10] In the great circle path, for each SIP, we calculate the onset time at the trial center by

$$T_{Ck} = T_{Ak} - D_{Rk}/V_R,$$

where D_{Rk} is the great circle distance of the kth SIP to the trial center. The similar procedure is employed for various average radial speeds to find the optimal onset time and CID origin location.

[11] Alternatively, our beam-forming technique, using the estimated travel times and the distances from the trial center to the SIPs, calculates the mean propagation speed and the standard deviation for each trial center (grid point) (Figure 1). Here, we simply assume the CID propagating along the great circle path, subtract the estimated onset time T_o from the observed arrival time T_{Ak} to obtain the estimated travel time at the kth SIP, and compute the speed V_{Rk} by

$$V_{Rk} = D_{Rk}/(T_{Ak} - T_o),$$

where D_{Rk} is the great circle distance between a trial center to the kth SIP. Thus, we calculate the mean speed and the standard deviation of the 14 SIPs for the trial center. We again repeat this procedure through the whole (global) grid points (trial centers) and draw contours of the standard deviations to find the disturbance origin on the Earth surface. To obtain the optimal result of the origin, we try various estimated onset times. In principle, the calculations of our two techniques simply need as limited as 3 CIDs to derive the propagation speed and disturbance origin.

3. Observation and Result

[12] A large earthquake occurred in the center region of Taiwan on 20 September 1999 at 17:47 UT (21 September, 01:47 LT). The epicenter was near the small country town of Chi-Chi (23.87°N, 120.75°E) (see Figure 2). Geologists from the National Central University in Taiwan have been in the field and report scarps with vertical offsets of 2–3 m along a 60 km north-south stretch of the Chelongpu fault (http://www.rcep.dpri.kyoto-u.ac.jp/~sato/taiwan/index.html). At several locations in the northern part of the faulted region, there are estimated displacements of 8 m. Because Taiwan borders the East China Sea, Philippine Sea, South China Sea, and Taiwan Strait, and it is difficult and inefficient to induce acoustic gravity waves on the sea surface, the CIDs triggered by the large vertical solid earth motions of the Chi-Chi earthquake most likely either traveled vertically upward reaching the ionospheric height and then horizontally reaching the SIPs or propagated radially from the epicenter directly to the SIPs (Figure 1).

[13] Figure 2 illustrates the locations of the epicenter, the Chelongpu fault as well as the ground-based GPS receivers and the associated SIPs used for this investigation. Note that the SIP locations are marked at the arrival (ticking) times, identified as the first data point suddenly and significantly deviating from its trend, of the CIDs. Figure 3 illustrates temporal variations of the TEC and dTEC, and the associated distance to the epicenter versus the travel time of each SIP. Two parallel slopes are shown in Figure 3c, one being the fitted least squares of the 14 CID arrival times and the other going through the earthquake onset time, and the time difference between the two lines show that the average horizontal and vertical speeds are about 1.5 ± 0.2 and 0.7 km/s, respectively. It can be seen that when traveling away from the epicenter, the associated energies (square of the one half of ridge-to-trough range) and periods (two times of the ridge-to-trough time interval) of the CIDs significantly decrease and generally increase, respectively (see Figures 4a and 4b). These indicate that the Chi-Chi CID is triggered by either a point or a line source, and the atmosphere acts as a low pass filter which results in the higher frequency CIDs being damped faster when they travel away from the origin.

[14] In both the ray-tracing and beam-forming calculations, we have tested onset times from 17:40 to 17:55 UT

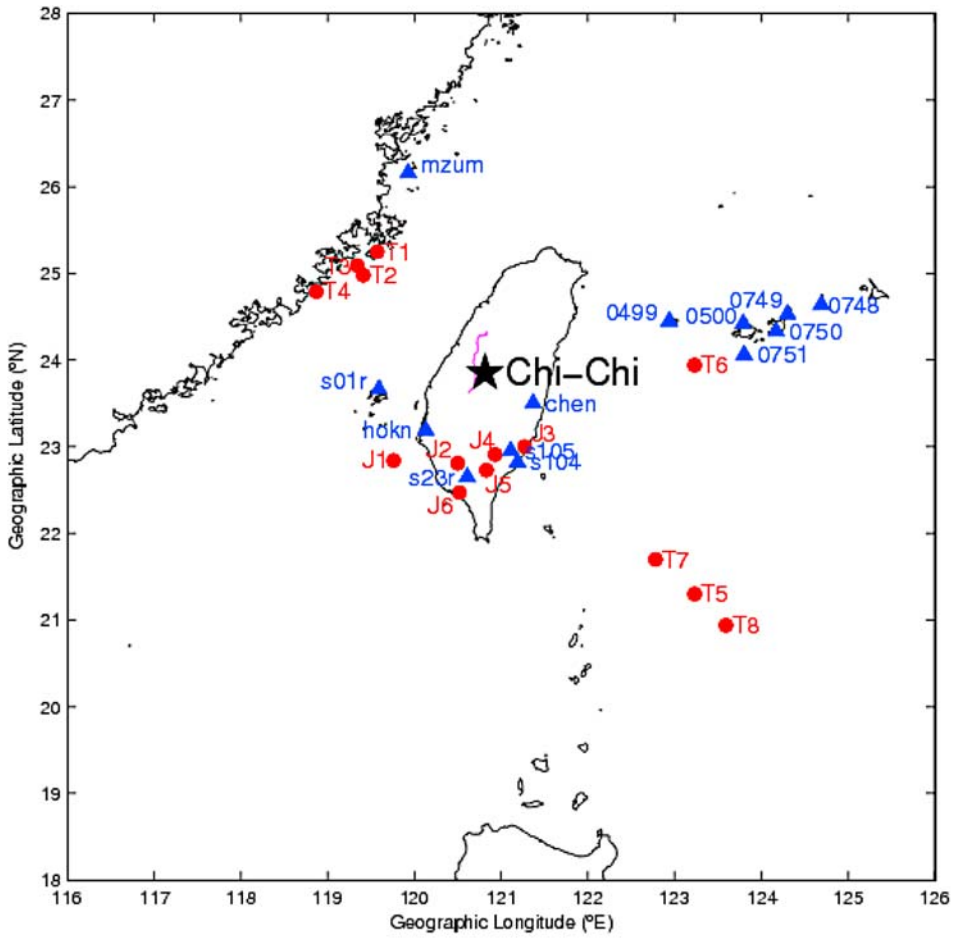

Figure 2. Locations of the epicenter of the Chi-Chi earthquake (star) and the Chelongpu fault (purple curves) as well as ground-based GPS receivers (triangles) and CIDs detected by the space seismometers at the SIPs (solid dots). The characters T1 to T8 are the SIPs on the slant paths of GPS satellite signals to receivers chen, s104, s105, s23r, mzum, s01r, hokn, s23r in Taiwan, while J1 to J6 are those to receivers 0499, 0500, 0748, 0749, 0750, 0751 in Japan. The corresponding time series of dTEC as well as the associated ground-based receiver and GPS satellite number are given in Figure 3.

and the trial center within 18°N–28°N and 116°E–126°E. For the ray-tracing search, we first adopted the two-segment path and tried the onset time with the horizontal speed V_H ranging from 1.1 to 1.9 km/s and the vertical speed V_V varying from 0.7 to 0.9 km/s. The optimal results can be obtained by finding the minimum values of the time difference between the calculated and observed onset times, the standard deviation, and/or the distance between the calculated center (disturbance origin) and the epicenter reported by the Center Weather Bureau (CWB) of Taiwan. Table 1 shows that V_H = 1.7 km/s and V_V = 0.7 km/s yield the identical onset time 17:47 UT and the minimum distance of 50.2 km (also see Figure 5a). We further take the great circle path and try the radial speed V_R from 0.5 to 1.7 km/s and find that the optimal results of the neatest onset time 17:47.5 UT and the minimum distance 40.4 km come with V_R = 0.7 and V_R = 0.9 km/s, respectively (Table 2). It can be seen that Figure 5b or 5c yields a better and/or clearer convergent contour than Figure 5a does. This suggests that the disturbances trigged by vertical surface motions of the Chi-Chi earthquake near the epicenter propagate radially into the ionosphere where they activate the CIDs.

[15] For the beam-forming technique, based on the results obtained above, we simply give the great circle path and

Figure 3. The temporal variations of ionospheric GPS TEC observed by each space seismometer during the Chi-Chi earthquake. (a) TEC versus time; (b) dTEC versus time, each y grid denotes 0.2 TECu/30 s (1 TECu = 10^{16} el/m^2); and (c) dTEC-time-distance from the space seismometer at the SIP to the epicenter, the dots denote the distance of the SIPs. The dashed line represents the onset time of the Chi-Chi earthquake. The dotted solid line and solid line are the fitted least squares of the 14 CIDs and the parallel going through the onset time, respectively. The number or characters before and after the # symbol denote the ground-based receiver and the GPS satellite number, respectively. T1–T8 and J1–J6 are the SIPs (also shown in Figure 2).

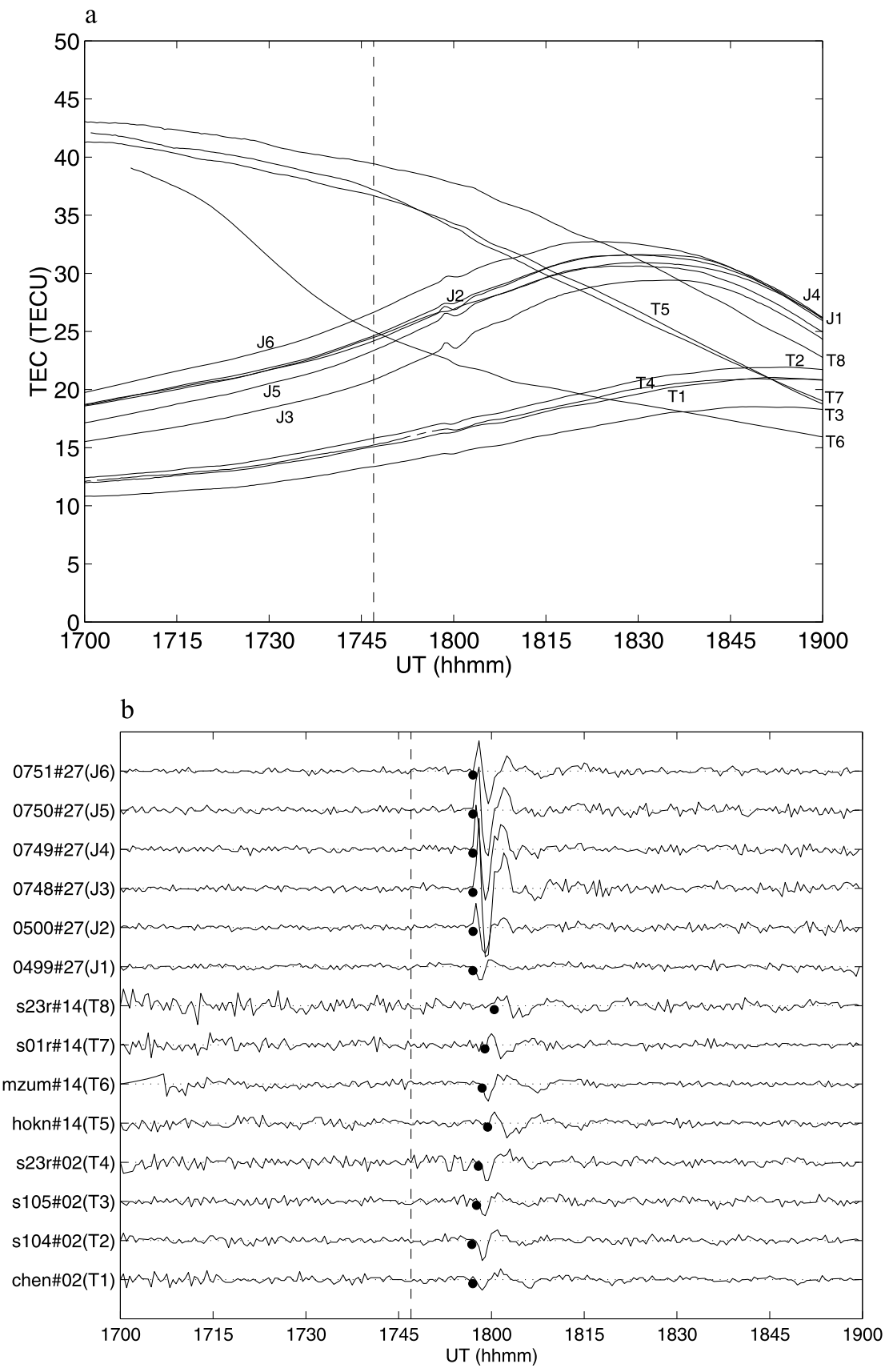
a
TEC (TECU)
UT (hhmm)
J1
J2
J3
J4
J5
J6
T1
T2
T3
T4
T5
T6
T7
T8
b
0751#27(J6)
0750#27(J5)
0749#27(J4)
0748#27(J3)
0500#27(J2)
0499#27(J1)
s23r#14(T8)
s01r#14(T7)
mzum#14(T6)
hokn#14(T5)
s23r#02(T4)
s105#02(T3)
s104#02(T2)
chen#02(T1)
UT (hhmm)

Figure 3

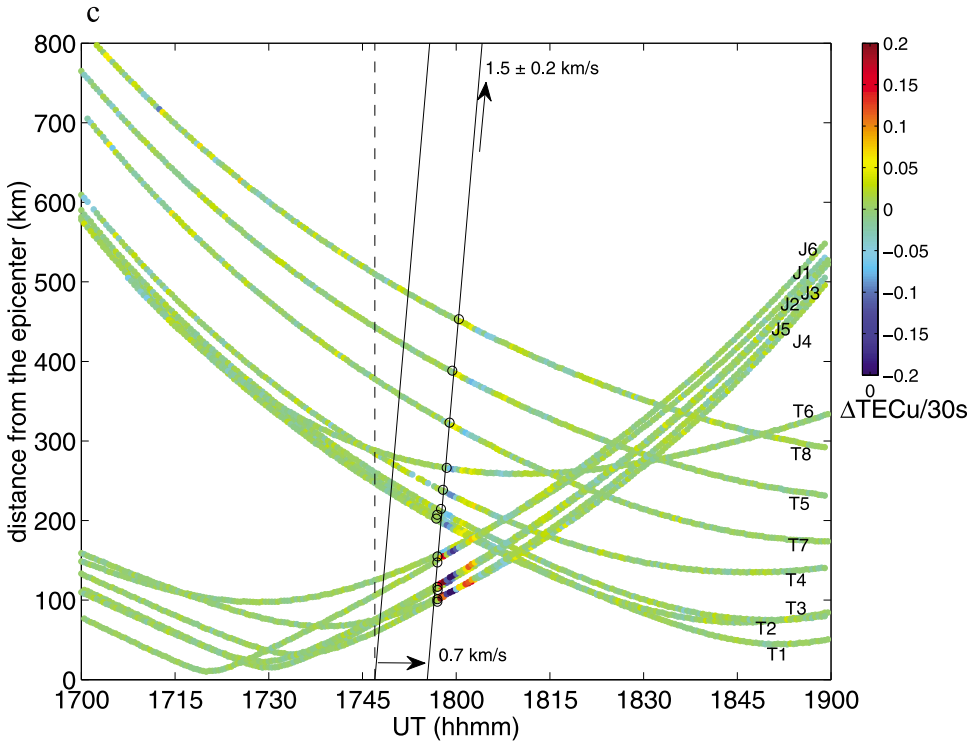

Figure 3. (continued)

compute the mean speed and standard deviation from each trial center to the 14 SIPs. Table 3 displays that the onset time at 17:49 UT yields the best result of the disturbance origin being located about 39 km north of the epicenter (Figure 5d). The optimal result of the mean radial speed and standard deviation is $V_R = 821 \pm 39$ m/s traveling away from the disturbance origin near the Earth surface and directly into the atmosphere and ionosphere.

4. Discussion and Conclusion

[16] *Davies* [1990] shows that the Doppler shift is made of two parts: (1) a part due to the motion of the satellite with respect to the receiver and (2) a part due to the rate of change of the total electric content along the signal ray path (or the line-of-sight), which can be expressed by

$$\Delta f = f\mu v_l/c + (40.3/cf)\text{dTEC},$$

where f is the satellite transmitting frequency, μ is the refractive index, and v_l is the line-of-sight component of the satellite velocity. Due to ultra high frequency (UHF) signals transmitted by the GPS satellite, $\mu = 1$. Since the GPS satellites move relatively slowly, the Doppler shift mainly results from the CIDs, $\Delta f = (40.3/cf)$dTEC. Moreover, the ionosphere is assumed to be a thin shell at 350 km altitude. Thus, $\Delta f = (40.3/cf)$dTEC can be converted to the equivalent Doppler velocity of the shell at 350 km altitude,

$$v = (40.3/2f^2)\text{dTEC}.$$

Thus, dTEC = 1 TECu/30 s is corresponding to an ionospheric layer at 350 km altitude moving 300 m/s vertically in the downward direction. The wave energy density of CIDs in the ionosphere can be given as $E = 1/2\rho v_m^2$, where ρ is the neutral density at 350 km altitude and v_m is the maximum of v. Note $v_m = A\omega$, where A and ω, denote the amplitude and angular frequency of the CIDs.

[17] The most pronounced ridge-to-trough in the Chi-Chi CIDs, which can be found in the fluctuation of 0748#27(or J3) in Figure 3b, has an amplitude (or 1/2 ridge-to-trough)

Figure 4. The characteristics of the CIDs triggered by the Chi-Chi earthquake. (a) The square of the maximum range of ridge-to-trough (or four times of the corresponding wave energy) of the CID versus the distance from the epicenter to the associated SIP. Open circle denotes three influentials, T1, T3, and T9. The dotted and solid curves are the fitted regression lines with and without three outliers. The fitted regression lines before and after removing the outliers are $E^{-3/2} = -671.9 + 2.4d$ and $E^{-3/2} = -1164.1 + 3.3d$, respectively. E and d denote the energy and distance. (b) The time duration of the CID ridge-to-trough (or 1/2 period) versus the travel time (time after the earthquake onset) at the associated SIP. The fitted regression line is $P = -34.5 + 0.22T$. P and T represent period and travel time.

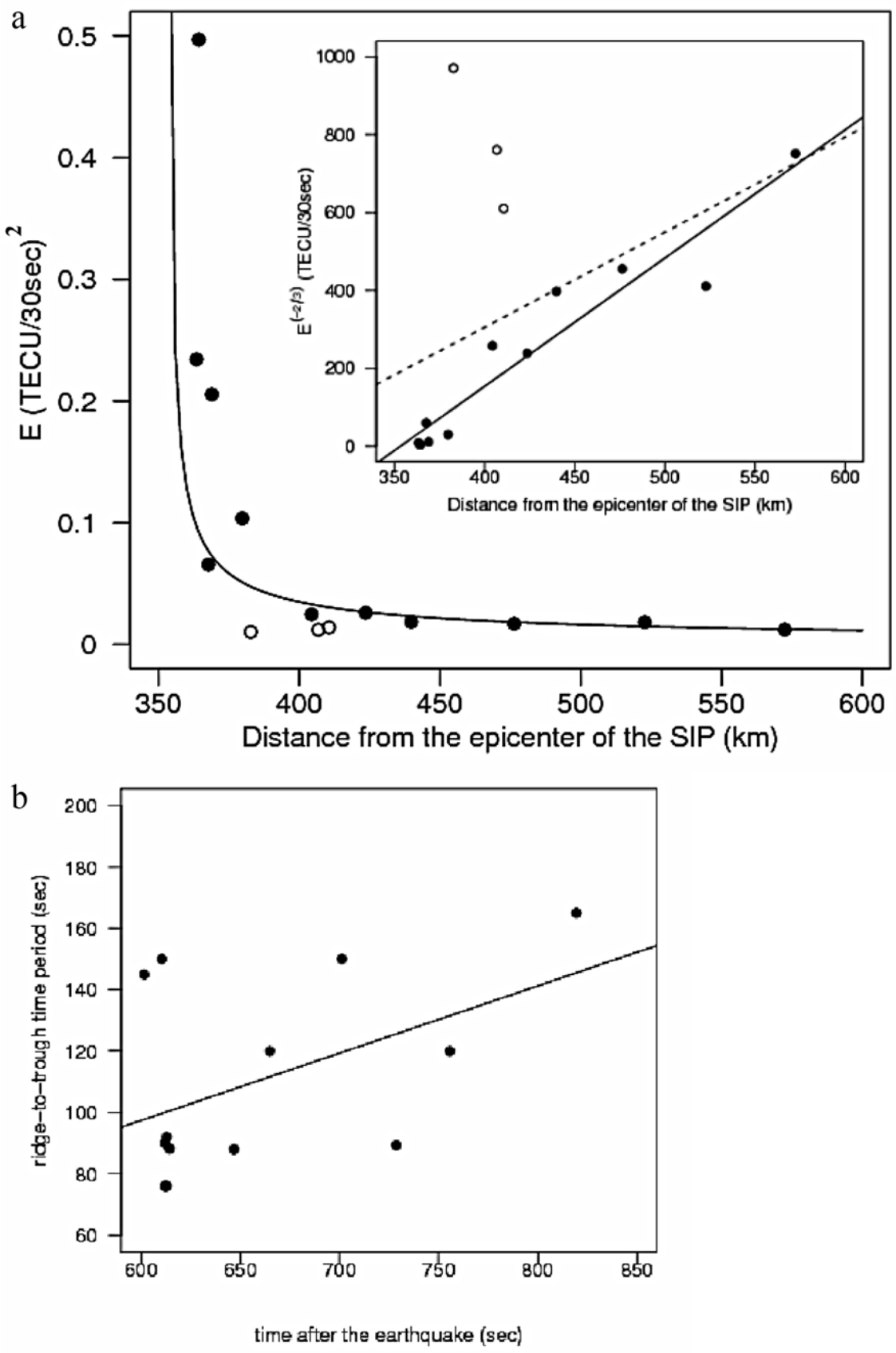
a
E (TECU/30sec)^2
Distance from the epicenter of the SIP (km)
E^(-2/3) (TECU/30sec)
Distance from the epicenter of the SIP (km)
b
ridge−to−trough time period (sec)
time after the earthquake (sec)

Figure 4

Table 1. The Ray-Tracing Search With the Two-Segment Path[a]

V_H (km/s)	V_V (km/s)	Onset (hh:mm)	Std (mm)	Distance (km)
1.1	0.7	17:45.5	0.6	67.0
1.3	0.7	17:46.0	0.5[b]	50.5
1.5	0.7	17:46.7	0.5[b]	50.5
1.7	0.5	17:43.0	0.6	50.2[b]
1.7	0.7	17:47.0[b]	0.6	50.2[b]
1.7	0.9	17:49.0	0.6	50.2[b]
1.9	0.7	17:47.0	0.6	57.0

[a]*VH*, horizontal velocity; *VV*, vertical velocity; Std, standard deviation.
[b]Closest onset time, the minimum Std in minute, or the minimum distance between the reported epicenter and the trial epicenter.

of about 0.33 TECu/30 s with a approximate period of 5 minutes (i.e., 2 times the time interval of ridge-to-trough). This means the equivalent maximum vibration velocity v_m being 100 m/s at 350 km altitude. Thus, if $\rho = 1.0 \times 10^{-11}$ kg/m^3 [*Kelly*, 1989], the CID energy density is about 5.0×10^{-11}J/m^3. Moreover, assuming the CID to be a cosine wave with a maximum velocity of about 100 m/s and a period of about 5 min, we then can obtain that the ionosphere has been the CID amplitude about 5.6 km. This shows due to the exponential decrease of neutral density with height that the amplification factor of the ionosphere relative to the near-Earth atmosphere is about 700 (= 5.6 km/8 m), which is much smaller than 50,000 induced by the *M* 9.3 Sumatra Earthquake Rayleigh waves [*Liu et al.*, 2006a] and 30,000 (or 17,000–43,000) triggered by the Indian Ocean tsunami [*Liu et al.*, 2006c]. Since the distance between the Sumatra Earthquake and Taiwan is about 3600 km, the arrivals of the Rayleigh waves in Taiwan are nearly simultaneous and coherent. Therefore, the simultaneously/coherently vertical motion of the whole Taiwan Island (as a plane wave source) results in a very effective amplification. Similarly, a large wavelength 120–240 km of the tsunami (again, nearly a plane source) has a rather coherent motion in the vertical direction, which also can give an effective amplification. Several models have been tested, and the best fit is that the energy (ridge-to-trough square) of the CID fluctuation is inversely proportional to the distance to the two-thirds power from the epicenter to the associated SIP. In zoomed plot of Figure 4a, the regression analysis for the whole 14 CIDs produces the correlation coefficient between energy and distance as 0.48. However, after removing the three influentials observed at T1, T3, and T9, the correlation coefficient is enhanced to be 0.96. Note that due to the very large vertical displacement of about 8 m occurring near the north part of the fault zone, it simply acts as a line source. Meanwhile, although the linear correlation of about 0.49 is not significant, the CID propagating the longer distance generally has the greater period (Figure 4b).

[18] *Davies* [1990] concludes that the speeds of CIDs induced by the Rayleigh waves and by the seismo-acoustic waves near the Earth's surface are about 3.5 km/s and about 300 m/s (or 0.3 km/s), respectively. The optimal results of the ray-tracing and beam-forming searches in the tables and figures show that the average propagating velocity is V_R = 0.7–0.9 km/s radially in the direction away from the epicenter, which suggests that the observed CIDs are neither triggered by the Chi-Chi Rayleigh waves nor seismo-acoustic waves. To have a better understanding in the Chi-Chi CID propagation, we adopt the 1D vertically stratified model of *Artru et al.* [2004, 2005] in our ray-tracing search. Based on the above models up to 300 km altitude, the average speed is about 0.5 km/s. We first test with the great circle path, which provides data similar to that in Table 2. It is found that the average speed V_R = 0.5 km/s estimated from the models results in the calculated onset time 17:43.0 UT +/−0.8 min, and the distance difference between the calculated origin and the reported epicenter is 63 km. Note that the calculated onset time is much earlier than that reported at 17:47 UT, and the average speed 0.5 km/s is slower than the earlier optimal results 0.7–0.9 km/s. To incorporate the calculated onset time approaching the observed one, we have to shorten the traveling time by assuming that the CIDs vertically take off from the ground, reach 350 km altitude, and then horizontally travel away, that is the CID taking the two-segment path. The velocity models is constructed by subdividing the speeds in the model in *Artru et al.* [2004, 2005] into six different ranges between 0 and 300 km altitude but in the seventh range vary the speed at 350 km altitude from 1.1 to 3.5 km/s (the speeds are linearly interpolated between the altitude ranges). Table 4 shows that the calculated onset times are still constantly earlier than the reported one 17:47 UT, even though the horizontal speed is assumed to be 3.5 km/s at 350 km altitude. This indicates that the Chi-Chi CID travels faster than the speeds reported by *Artru et al.* [2004, 2005] and/or their speeds might be underestimated. We further use the above constructed velocity model and apply *Lee and Lahr* [1972] for computing the source location of the Chi-Chi CID on the ground. It is found that the computed source location, 38 km north of the Chi-Chi epicenter, and the one obtained by our ray-tracing search with the great circle path are near identical; however, again the onset time of the computed 17:43 UT is earlier than that of the reported 17:47 UT. The agreement in the results derived by our ray-tracing search and *Lee and Lahr* [1972] confirm that the Chi-Chi CID travels faster than the sound speed. On the other hand, *Astafyeva et al.* [2009] show that due to the mixing of wave modes, shock-acoustic waves, and Rayleigh waves, the apparent velocity within 600–700 km from the epicenter is about 1 km/s. Since our SIPs are mainly over the ocean surface, the Chi-Chi CID is more likely to be induced by shock-acoustic waves than by its surface Rayleigh waves. In fact, the N-shape of TEC variations (i.e., compression-rarefaction waves) [*Astafyeva and Heki*, 2009] registered by satellite #27 over the Taiwan Island in Figure 3b indicate

Figure 5. The optimal results obtained by the ray-tracing technique and the beam-forming technique. Contours of the onset time standard deviations by the ray-tracing technique. The velocity models: (a) V_H = 1.7 km/s, V_V = 0.7 km/s, (b) V_R = 0.7 km/s, and (c) V_R = 0.9 km/s. (d) Contours of the speed standard deviations for the tested onset time at T_o = 17:49 UT by the beam forming technique. The epicenter reported by the CWB and the disturbance origin near the Earth surface calculated by the technique are denoted by the stars and the solid squares, respectively. Note that the solid square is the minimum value of the lower standard deviation contour. The dots represent the SIPs. The open star is the epicenter computed by using *Lee and Lahr* [1972].

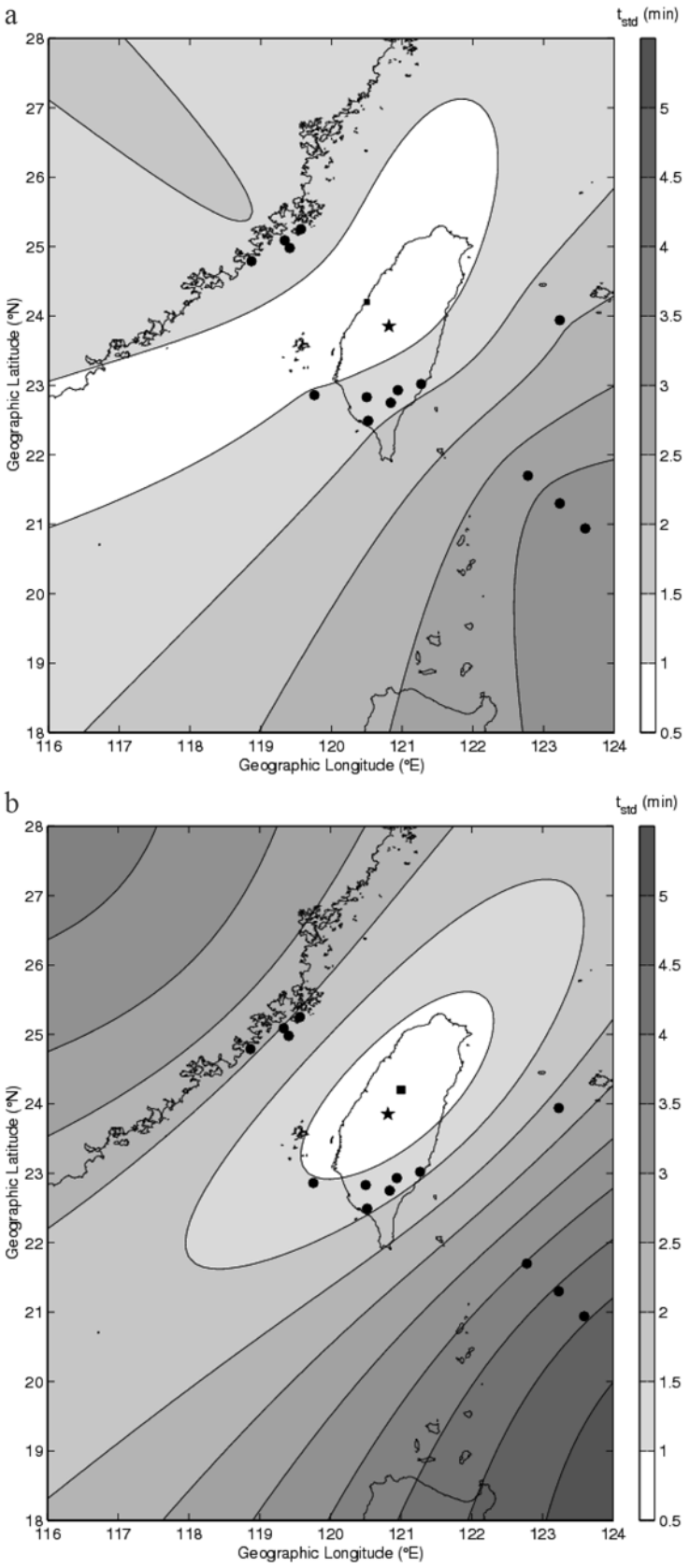
a
b
t_{std} (min)
Geographic Latitude (°N)
Geographic Longitude (°E)
28
27
26
25
24
23
22
21
20
19
18
116
117
118
119
120
121
122
123
124
5
4.5
4
3.5
3
2.5
2
1.5
1
0.5

Figure 5

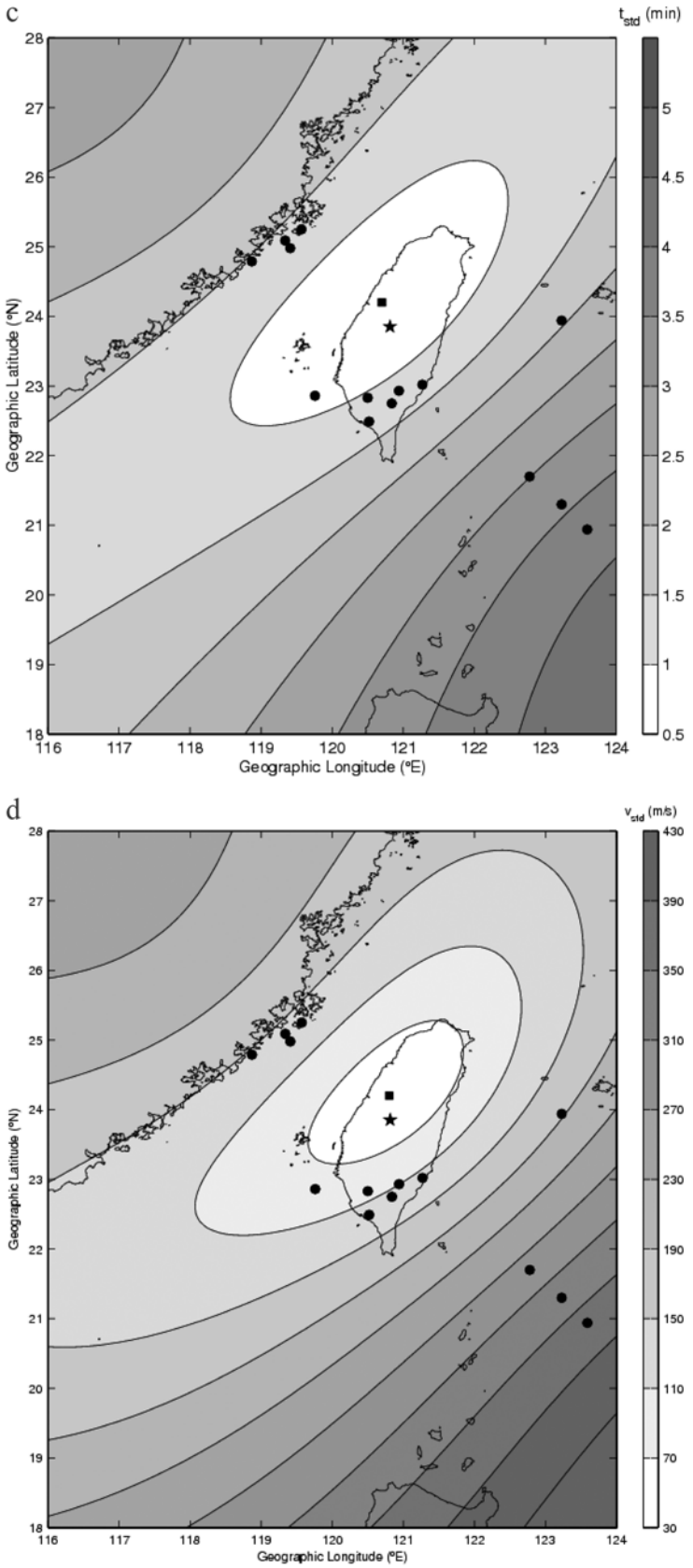

Figure 5. (continued)

Table 2. The Ray-Tracing Search With the Great Circle Path[a]

V_R (km/s)	Onset (hh:mm)	Std (mm)	Distance (km)
0.5	17:43.0	0.8	63.0
0.7	17:47.5[b]	0.5[b]	43.0
0.9	17:49.8	0.5[b]	40.4[b]
1.1	17:51.0	0.5[b]	57.0
1.3	17:52.0	0.6	80.0
1.5	17:52.8	0.6	105
1.7	17:53.3	0.7	133

[a]V_R, radial velocity.
[b]Closest onset time, the minimum standard deviation (Std) in minute, or the minimum distance between the reported epicenter and the trial epicenter.

that the CID is most likely caused by propagating shock-acoustic waves. Furthermore, the optimal results of traveling in the radial direction in the atmosphere and ionosphere shown in Figures 5c and 5d also support the Chi-Chi CID to be associated with shock-acoustic waves.

[19] It is known that the acoustic gravity wave may show significant wind-filter effect during its upward propagation from the source in the lower atmosphere. As a result, the true source location might be different if there are strong horizontal neutral winds around where it propagates. To estimate the location difference between the true source and the computed one, we obtain the horizontal neutral winds in the troposphere from WINDFINDER.COM (http://www.windfinder.com/windstats/windstatistic_tainan_airport.htm), in the stratosphere and mesosphere from the SKYHI model (http://www.nersc.gov/news/annual_reports/annrep98/hamilton.html), and in the thermosphere from the horizontal wind model HWM2007 (cf. *Alken et al.*, 2008). It is found that the horizontal neutral winds in the troposphere, stratosphere-mesosphere, and thermosphere are about 4, 50, and 70 m/s, which are much smaller than the average propagating velocity 700–900 m/s computed in this study. It takes 600–800 s for the CIDs traveling from the epicenter to the ionosphere at an altitude of 350 km altitude (Figures 3 and 4b). Assuming the horizontal wind in the atmosphere at an altitude of 0–400 km yields a top speed 70 m/s in the same direction, we find that the error of locating the CID origin on the Earth surface is 56 km (= 70 m/s × 800 s) which is within the minimum standard error shown in Figures 5a–5d.

[20] It is interesting to note in Figure 5 that the CID origins are located on Taiwan Island about 40-50 km northwest (or north) of the epicenter, which coincides with the location of the maximum displacements of 8 m reported by the seismologists (http://www.rcep.dpri.kyoto-u.ac.jp/~sato/taiwan/index.html). The coincidence further confirms that the CIDs are induced by the large and sudden vertical surface motions

Table 3. The Beam Forming Search With the Great Circle Path[a]

T_o (hh:mm)	V_R (km/s)	Std (m/s)	Distance (km)
17:46	0.61	31[b]	48
17:47	0.64	33	43
17:48	0.74	36	40
17:49	0.82	39	39[b]
17:50	0.93	48	40
17:51	1.07	62	44

[a]T_o, estimated onset time; V_R, radial velocity; Std, standard deviation.
[b]Closest onset time, the minimum Std in minute, or the minimum distance between the reported epicenter and the trial epicenter.

Table 4. The Ray-Tracing Search With the Speed Model and the Two-Segment Path[a]

V_H (km/s)	V_V (km/s)	Onset (hh:mm)	Std (mm)	Distance (km)
1.1	0.5	17:42	0.6	67
1.3	0.5	17:43	0.5[b]	51
1.5	0.5	17:43	0.5[b]	51
1.9	0.5	17:44	0.6	57
2.1	0.5	17:44	0.6	65
2.3	0.5	17:44	0.7	78
2.5	0.5	17:44	0.7	87
3.5	0.5	17:45	0.6	120

[a]V_H, horizontal velocity; V_V, vertical velocity; Std, standard deviation.
[b]Closest onset time, the minimum Std in minute, or the minimum distance between the reported epicenter and the trial epicenter.

of the Chi-Chi earthquake. In conclusion, a combination of the ionospheric GPS TEC observation and standard seismological techniques, the ray-tracing and beam-forming searches, can be used to locate the origin and evaluate the propagation of CIDs triggered by a strong earthquake. The Chi-Chi CIDs are mainly attributed to shock-acoustic waves.

[21] **Acknowledgments.** This paper was initiated when JYL and HFT visited the institute of Earth Sciences, Academia Sinica during January–April, 2000. The GPS data are obtained from the Ministry of Interior of Taiwan, Institute of Earth Sciences at Academia Sinica of Taiwan, and the Geographical Survey Institute of Japan. The earthquake catalog is obtained from the Central Weather Bureau of Taiwan. This research was partially supported by the Ministry of Education under Grant 91-N-FA07-7-4 for the iSTEP project of the National Central University.

[22] Zuyin Pu thanks Elvira Astafyeva and another reviewer for their assistance in evaluating this paper.

References

Afraimovich, E. L., N. P. Perevalova, A. V. Plotnikov, and A. M. Uralov (2001), The shock-acoustic waves generated by earthquakes, *Ann. Geophys.*, *19*, 395–409.

Afraimovich, E. L., E. I. Astafieva, and V. V. Kirushkin (2006), Localization of the source of ionospheric disturbance generated during an earthquake, *Int. J. Geomagn. Aeron.*, *6*, GI2002, doi:10.1029/2004GI000092.

Alken, P., S. Maus, J. Emmert, and D. P. Drob (2008), Improved horizontal wind model HWM07 enables estimation of equatorial ionospheric electric fields from satellite magnetic measurements, *Geophys. Res. Lett.*, *35*, L11105, doi:10.1029/2008GL033580.

Artru, J., T. Farges, and P. Lognonne (2004), Acoustic waves generated from seismic surface waves: Propagation properties determined from Doppler sounding observations and normal-mode modeling. *Geophys. J. Int.*, *158*, 1067–1077.

Artru, J., V. Ducic, H. Kanamori, P. Lognonne', and M. Murakami (2005), Ionospheric detection of gravity waves induced by tsunamis, *Geophys. J. Int.*, *160*, 840–848.

Astafyeva, E. I., and E. L. Afraimovich (2006), Long-distance traveling ionospheric disturbances caused by the great Sumatra-Andaman earthquake on 26 December 2004, *Earth Planets Space*, *58*, 1025–1031.

Astafyeva, E. I., and K. Heki (2009), Dependence of waveform of near-field coseismic ionospheric disturbances on focal mechanisms, *Earth, Planets Space*, *61*, 939–943.

Astafyeva, E., K. Heki, V. Kiryushkin, E. Afraimovich, and S. Shalimov (2009), Two-mode long-distance propagation of coseismic ionosphere disturbances, *J. Geophys. Res.*, *114*, A10307, doi:10.1029/2008JA013853.

Blanc, E. (1985), Observations in the upper atmosphere of infrasonic waves from natural or artificial sources: A summary, *Ann. Geophys.*, *3*, 673–688.

Bolt, B. A. (1964), Seismic air waves from the great 1964 Alaskan earthquake, *Nature*, *202*, 1094–1095.

Calais, E., and J. B. Minster (1995), GPS detection of ionospheric perturbations following the January 17, 1994, Northridge earthquake, *Geophys. Res. Lett.*, *22*, 1045–1048.

Davies, K. (1990), *Ionospheric Radio*, Peter Peregrinus, London.

Davies, K., and D. M. Baker (1965), Ionospheric effects observed around the time of the Alsaka earthquake of March 28, 1964, *J. Geophys. Res.*, *70*, 1251–1253.

Ducic, V., J. Artru, and P. Lognonné (2003), Ionospheric remote sensing of the Denali Earthquake Rayleigh surface waves, *Geophys. Res. Lett.*, *30*(18), 1951, doi:10.1029/2003GL017812.

Fowles, R. F., and G. L. Cassiday (1999), *Analytical Mechanics*, 6th ed., 484 pp., Saunders College Publishing, Philadelphia.

Heki, K., and J. Ping (2005), Directivity and apparent velocity of the cosemic ionospheric disturbances observed with a dense GPS array, *Earth Planet Sci. Lett.*, *236*, 845–855.

Huang, B. S., K. C. Chen, H. Y. Yen, and Z. X. Yao (1999), Re-examination of the epicenter of the 16 September 1994 Taiwan Strait earthquake using the beam-forming method. *Terr. Atmos. Oceanic Sci.*, *10*, 529–542.

Jung, T. K., J. Y. Liu, H. F. Tsai, B. S. Huang, C. H. Lin, S. B. Yu, and Y. S. Yeh (2006), Ionospheric disturbances triggered by the Mw7.6 earthquake off the coast of El Salvador on 13 January 2001, *Terr. Atmos. Oceanic Sci.*, *17*, 345–351.

Kelly, M. C. (1989), *The Earth's Ionosphere, Plasma Physics and Electrodynamics*, 847 pp., Academic Press, San Diego.

Kiryushkin, V. V., and E. L. Afraimovich (2007), Determining the parameters of ionospheric perturbation caused by earthquakes using the quasi-optimum algorithm of spatiotemporal processing of TEC measurements, *Earth Planets Space*, *59*, 267–278.

Lee, W. H. K., and J. C. Lahr (1972), HYPO71: A computer program for hypocenter, magnitude and first motion pattern of local earthquakes, U.S. Geol. Surv. open file report.

Lee, W. H. K., and S. W. Stewart (1981), *Principles and Applications of Microearthquake Networks*, Academic Press, San Francisco.

Leick, A. (1995), *GPS Satellite Surveying*, 560 pp., John Wiley, New York.

Leonard, R. S., and R. A. Barnes (1965), Observations of ionospheric disturbances following the Alaska earthquake, *J. Geophys. Res.*, *70*, 1250–1253.

Liu, J. Y., H. F. Tsai, and T. K. Jung (1996), Total electron content obtained by using the global positioning system, *Terr. Atmos. Oceanic Sci.*, *7*, 107–117.

Liu, J. Y., C. H. Lin, H. F. Tsai, and Y. A. Liou (2004), Ionospheric solar flare effects monitored by the ground-based GPS receivers: Theory and observation, *J. Geophys. Res.*, *109*, A01307, doi:10.1029/2003JA009931.

Liu, J. Y., Y. B. Tsai, S. W. Chen, C. P. Lee, Y. C. Chen, H. Y. Yen, W. Y. Chang, and C. Liu (2006a), Giant ionospheric disturbances excited by the M9.3 Sumatra earthquake of 26 December 2004, *Geophys. Res. Lett.*, *33*, L02103, doi:10.1029/2005GL023963.

Liu, J. Y., Y. B. Tsai, K. F. Ma, Y. I. Chen, H. F. Tsai, C. H. Lin, M. Kamogawa, and C. P. Lee (2006b), Ionospheric GPS total electron content (TEC) disturbances triggered by the 26 December 2004 Indian Ocean tsunami, *J. Geophys. Res.*, *111*, A05303, doi:10.1029/2005JA011200.

Liu, J. Y., C. H. Lin, Y. I. Chen, Y. C. Lin, T. W. Fang, C. H. Chen, and Y. C. Chen, and J. J. Hwang (2006c), Solar flare signatures of the ionospheric GPS total electron content, *J. Geophys. Res.*, *111*, A05308, 10.1029/2005JA011306.

Otsuka, Y., N. Kotake, T. Tsugawa, K. Shiokawa, T. Ogawa, S. Saito Effendy, M. Kawamura, T. Maruyama, N. Hemmakorn, and T. Komolmis (2006), GPS detection of total electron content variations over Indonesia and Thailand following the 26 December 2004 earthquake, *Earth Planet Space*, *58*, 159–165.

Pokhotelov, O. A., M. Parrot, E. N. Fedorov, V. A. Pilipenko, V. V. Surkov, and V. A. Gladychev (1995), Response of ionosphere to natural and man-made acoustic sources, *Ann. Geophys.*, *13*, 1197–1210.

Row, R. V. (1967), Acoustic-gravity waves in the upper atmosphere due to a nuclear detonation and an earthquake, *J. Geophys. Res.*, *72*, 1599–1610.

Sardón, E., A. Rius, and N. Zarraoa (1994), Estimation of the transmitter and receiver differential biases and the ionospheric total electron content from global positioning system observation, *Radio Sci.*, *29*, 577–589.

Tanaka, T., T. Tchinose, T. Okusawa, T. Shibata, Y. Sato, C. Nagasawa, and T. Ogawa (1984), HF Doppler observations of acoustic waves exhibited by the Urakawa-Oki earthquake on 21 March 1982, *J. Atmos. Terr. Phys.*, *46*, 233–245.

Tsai, H. F., and J. Y. Liu (1999), Ionospheric total electron content response to solar eclipses, *J. Geophys. Res.*, *104*, 12657-12668.

Yuen, P. C., P. F. Weaver, R. K. Suzuki, and A. S. Furumoto (1969), Continuous traveling coupling between seismic waves and the ionosphere evident in May 1968 Japan earthquake data, *J. Geophys. Res.*, *74*(9), 2256–2264.

Y. I. Chen, Institute of Space Statistics, National Central University, Chung-Li 320, Taiwan.

B. S. Huang, C. H. Lin, Y. H. Yeh, and S. B. Yu, Institute of Earth Sciences, Academia Sinica, Taipei 115, Taiwan.

M. Kamogawa, Department of Physics, Tokyo Gakugei University, 4-1-1 Nukuikitamachi, Koganei-shi, Tokyo, Japan.

C. H. Lin, Department of Earth Science, National Cheng Kung University, Tainan 701, Taiwan.

J. Y. Liu, Institute of Space Science, National Central University, Chung-Li, Taiwan. (jyliu@jupiter.ss.ncu.edu.tw)

H. F. Tsai, Center Weather Bureau, Taipei 100, Taiwan.